**Structural Engineering and Mechanics**, *Vol. 73, No. 2 (2020) 167-179*
DOI: https://doi.org/10.12989/sem.2020.73.2.167


# A simplified method for evaluation of shear lag stress in box T-joints considering effect of column flange flexibility

Piseth Doung* and Eiichi Sasaki[a]

*Department of Civil and Environmental Engineering, Tokyo Institute of Technology, 2-12-1 Ookayama, Meguru-ku, Tokyo 152-8552, Japan*

*(Received March 27, 2019, Revised August 2, 2019, Accepted October 5, 2019)*

**Abstract.** This study provides a simplified method for the evaluation of shear lag stress in rectangular box T-joints. The occurrence of shear lag phenomenon in the box T-joint generates stress concentration localized at both web-flange junctions of the beam, which leads to cracking or failure in the weld region of the joint. To prevent such critical circumstance, peak stress at the weld region is required to be checked during a preliminary design stage. In this paper, the shear lag stresses in the T-joints were evaluated using least-work solution in which the longitudinal displacements of the beam flange and web were presumed. The evaluation process considered particularly the effect of column flange flexibility, which was represented by an axial spring model, on the shear lag stress distribution. A simplified method for stress evaluation was provided to avoid solving complex mathematical problems using a stress modification factor $\beta_s$ from a parametric study. The results showed that the proposed method was valid for predicting the shear lag stress in the box T-joints manually, as well compared with finite element results. The results are further summarized, discussed, and clarified that more flexible column flange caused higher stress concentration.

**Keywords:** box T-joints; column flange flexibility; diaphragms; shear lag; stress concentration

## 1. Introduction

Box section steel members have been extensively used in various engineering practices including buildings, bridges, and other mechanical and agricultural equipment (Moazed *et al*. 2009). For building, an exterior column in framing system creates a typical joint known as T-joint, in which the forces are geometrically transmitted to one side of the column. For a rectangular box T-joint, shear lag problem raised concern over the stress concentration localized at the junctions between the beam flange and web, which possibly cause an unexpected failure of the weld at the joint region. Therefore, checking the stress concentration at the joint region is required in a preliminary design stage. The stress concentration due to shear lag in a box member can be evaluated using several potential techniques, such as least-work solution (Reissner 1941, 1946, Dezi and Mentrasti 1985, Chang and Zheng 1987, Lee *et al*. 2001, Lin and Zhao 2011), closed-form solution (Chen *et al.* 2014, Zhou *et al.* 2012), harmonic analysis (Winter 1940, Kristek *et al.* 1990, Tahan *et al.* 1997), or finite element method (FEM). Each method, however, has not yet provided a more simplified application to minimize calculation time for the box members in the preliminary design stage. For instance, FEM is one of the most powerful computation methods to evaluate the characteristic terms with reliable approximate values. Nonetheless, the approach requires comprehensive modeling and costly computation time and memory sizes. Currently, the least-work solution is one of the simplest methods to conveniently predict the stress due to shear lag. Such that issue has been considered, a challenge to develop an easy and accurate stress evaluation approach for the box members has been conducted.

Shear lag in a box T-joint deals with the stress concentration at both edges of the beam or column flange. Moreover, the phenomenon affects to decrease the lateral stiffness of the structure due to the growth of the structural deflection (Mohammadnejad and Kazemi 2018). The peak stress is normally critical to cause cracking or failure in the weld region under cyclic loads (Fadden and McCormick 2013). The examples of the failure had been observed in Japan during the great Hanshin earthquake in 1995; there were cracking and brittle failures occurred in the weld region of the knee joint in steel frame pier (Miki and Sasaki 2005). Afterward, the required peak stress in the weld region of the joint had been numerously assessed using both FEM and experiment. The assessment was also conducted for comparison with the existing manual method which was utilized based on Okumura' stress equation (Okumura and Ishizawa 1968). The comparison results showed that the existing approach was not alternative enough to evaluate the peak stress for the preliminary design stage of the knee joint. The error was much motivated to consider a revisit of the existing manual calculation of the peak stress due to shear lag. An extensive study by Hwang *et al*. (2004) revealed that predicting peak stress using a cantilever beam model for the knee joint was less sensitive as the shear lag stress went up twice higher than the stress given by Okumura' equation. However, Hwang *et al.* failed to clarify the effects

*Corresponding author, Ph.D. Candidate
E-mail: doung.p.aa@m.titech.ac.jp
[a] Associate Professor



ISSN: 1225-4568 (Print), 1598-6217 (Online)

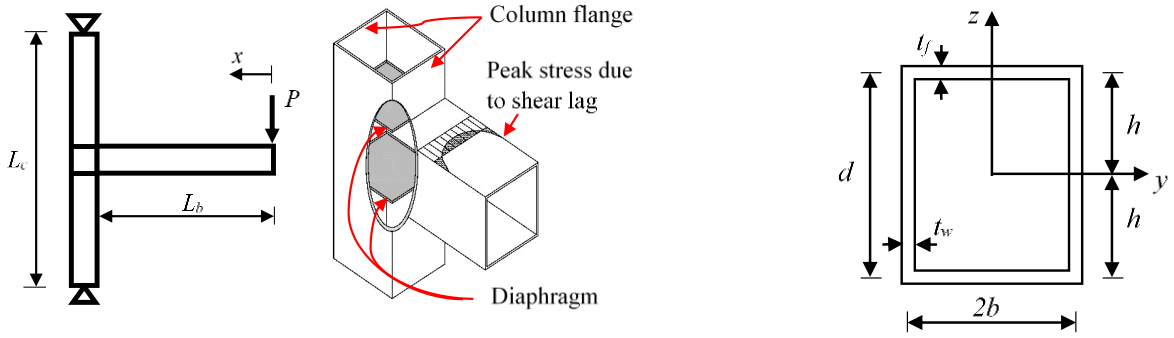


(a) Box T-joint with diaphragm (b) Beam section geometry

Fig. 1 Box T-joint configuration

of column flange flexibility and shear lag in the web on the stress distribution in the beam flange.

In the design codes, such as ANSI/AISC 360-10 (2010), Eurocode 3 (2008), and CIDECT 9 (2004), the shear lag phenomenon in a box T-joint is considered when the beam-to-column flange width ratio ($\beta$) is greater than 0.85. The effective width of the beam flange is utilized to evaluate the joint's strength and is calculated using Eq. (1) below.

$$b_e = \frac{10}{(b_c/t_c)}\left(\frac{F_{yc}t_c}{F_{yb}t_b}\right)b_b \quad (1)$$

where $b_c$ and $t_c$ denote the column flange width and thickness, respectively. $F_{yc}$ refers to the yield stress of the column. $t_b$, $b_b$, and $F_{yb}$ express the beam flange thickness, width, and yield stress, respectively. The application of the box T-joint in the design codes is available for the box beam-to-column connection, which diaphragm (continuity plate) is not used. The presence of the diaphragm increases the rigidity for the connection, and meanwhile, the stress in the beam flange gets affected. The dismissal of considering the effects of column flange flexibility, which is able to generate the initial longitudinal displacement of the beam flange, may deliver an under-estimated stress distribution in the beam flange. Therefore, this study emphasizes the effects of the column flange flexibility on shear lag stress in the T-joints including the consideration of shear lag in the beam web. A simplified method to evaluate the shear lag stress is also provided to serve as an alternative preliminary design for the required stress in the beam flange. The configurations of the box T-joint are illustrated in Fig. 1.

## 2. Column flange flexibility

The prediction of shear lag stress in a box beam using least-work solution is associated with assuming a longitudinal displacement of the beam flange and web containing an unknown displacement density and applying boundary conditions to find a general solution for the corresponding parameters. Various boundary conditions for the box beam were specified by Reissner (1941, 1946). However, the application of boundary conditions for the T-joint is not yet available. The least-work solution confirmed that the initial longitudinal displacement of the beam flange causes the stress concentration at the flange edge and the lowest at the mid-width of the beam flange. In this study, a boundary effect known as column flange flexibility (with/without diaphragm), which generates an initial displacement for the beam flange, was considered.

### *2.1 Box T-joint without diaphragms*

In the design codes, the strength of a box T-joint without diaphragm subjected to in-plane bending can be evaluated through three limit states, such as column flange plastification, column web yielding, and local yielding of beam flange. However, only column web yielding and local yielding of the beam are governed when the beam-to-column flange width ratio $\beta \geq 0.85$. When this case is considered, the effective width method is utilized to calculate the flexural strength of the joint assuming that stress uniformly distributed along the effective width of the beam flange.

The prediction of effective width requires the known function of stress distribution (Tenchev 1996). For that reason, stress in the beam flange at the joint had to be primarily delivered. The stress evaluation using the least-work solution requires boundary conditions to fulfill the solution for the longitudinal displacement of the beam flange. Therefore, the effect of the column flange flexibility on the stress distribution was mainly concerned. The column flange is flexible at the mid-width and becomes fixed at the edge of the flange. The maximum displacement under the transmitted force by the beam flange can be appraised using the plate theory. The column flange was assumed to be a rectangular plate of infinite length with both fixed-supported edges. Such the transmitted load by the beam flange is innately non-uniform, a uniform load distribution on the effective width was assumed. The modeling of the column flange under the force of the beam flange is depicted in Fig. 2.

A relevant study on the deflection of the rectangular plate of infinite length with simply-supported edges can be found in Timoshenko's publication (Timoshenko and Woinowsky-Krieger 1987). Under a load of length $u$ uniformly distributed along a portion of $x$-axis, the deflection of the plate is expressed as:

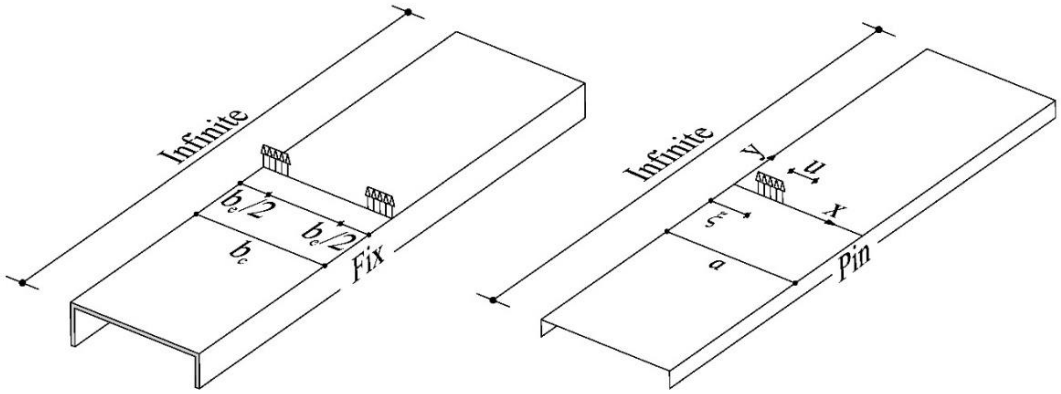


Fig. 2 Column flange bending

$$w_s = \frac{q_0 a^3}{\pi^4 D}\sum_{m=1}^{\infty}\frac{1}{m^4}\sin\frac{m\pi\xi}{a}\ \sin\frac{m\pi u}{2a}\left(1+\frac{m\pi y}{a}\right) \times e^{-\frac{m\pi y}{a}}\ \sin\frac{m\pi x}{a} \tag{2a}$$

where the geometric dimensions $\xi$, $u$, and $a$ can be seen in Fig. 2b.

For the simply-supported plate of infinite length under effective load distributed as shown in Fig. 2, the values of $\xi$ and $u$ can be taken as $b_e/4$ and $b_e/2$, respectively. Hence, the deflection of the plate at $x = a/2$ and $y = 0$ can be deduced to

$$w_s = \frac{q_0 a^3}{\pi^4 D}\sum_{m=1}^{\infty}\frac{1}{m^4}\sin^2\frac{m\pi b_e}{4a}\ \sin\frac{m\pi}{2} \tag{2b}$$

The deflection of the plate can be generally simplified to an expression corresponding to a coefficient $\alpha$ as shown in Eq. (2c).

$$w_s = \alpha\frac{q_0 a^3}{D} \tag{2c}$$

where, $\alpha = \frac{1}{\pi^4}\sum_{m=1}^{\infty}\frac{1}{m^4}\sin^2\frac{m\pi b_e}{4a}\ \sin\frac{m\pi}{2}$,

and $D = \frac{Et_c^3}{12(1-\nu^2)}$

For the fixed-supported plate of infinite length under the effective load, the coefficient $\alpha$ can be obtained by modifying the simply-supported plate to a fixed-supported plate by a coefficient $r_k$. The coefficient $r_k$ represents the ratio of rigidity between the fixed and simply-supported plates and is expressed as follows.

$$r_k = \frac{(2\lambda_e^3 - \lambda_e^4)}{(\lambda_e^4 - 8\lambda_e^3 + 18\lambda_e^2 - 8\lambda_e + 2)} \tag{3}$$

where $\lambda_e$ denotes the ratio between $b_e$ and $a$. Hence, the deflection of the fixed-supported plate of infinite length under the effective load can be written as:

$$w_f = \alpha_f\frac{q_0 a^3}{D} \tag{4}$$

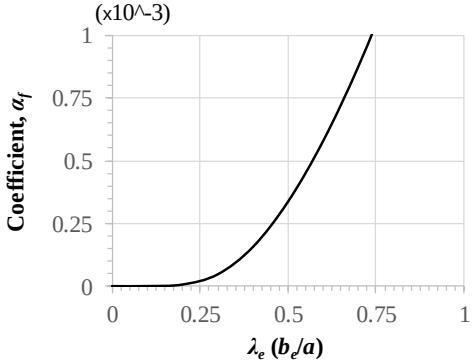


Fig. 3 Flexibility coefficient of column flange

where $\alpha_f = 2r_k\alpha$, in which the value 2 refers to the doubly-symmetric effective loads. The load transmitted from the beam flange $F_b$ ($F_b = q_0 a$) can be obtained by

$$F_b = \frac{M_b}{d_b} \tag{5}$$

where $M_b$ denotes the bending moment of the beam and $d_b$ is the distance between the centroid of the beam flanges. The flexibility coefficient $\alpha_f$ of the fixed-supported plate corresponding to the ratio $\lambda_e$ can be plotted corresponding to $\lambda_e$, as shown in Fig. 3 below. It was observed that $\alpha_f$ increased exponentially corresponding to the value of $\lambda_e$ from 0.25-1. This characteristic conveyed that the deflection of the column flange grew if the effective width of the beam flange increased and that affected the stress in the beam flange to grow as well.

### *2.2 Box T-joint with internal diaphragms*

A box T-joint may not provide sufficient strength as required to be a moment connection due to the flexibility of the column flange. The trendy choice for enhancing the performance of the box T-joint is to settle the diaphragms (continuity plates) into the joint (AIJ 2008, CIDECT 9 2004). The role of internal diaphragms in the box beam-to-column joint is crucial to contribute strength and stiffness to the joint because it creates high restraint against the deflection of the column flange under the transmitted load from the beam. More importantly, the internal diaphragm

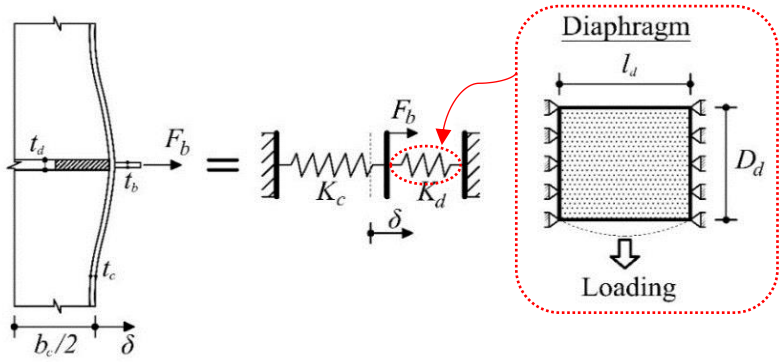


Fig. 4 Spring model for column flange and diaphragm

provides a significant strength increase in the joint when the width of the beam flange mismatches to that of the column flange ($\beta$ < 0.85). The internal diaphragms have also been seen in use for decades in box knee- and T-joints of bridge pier (JRA 2002, Tanebe 2005). The concern on stress concentration at the joint has been raised in discussion in the stress design method on the knee- and T-joints of the bridge piers. As the presence of the internal diaphragm increased the rigidity of the joint, evaluating the stress concentration was carried out assuming that the joint behaves similarly to a cantilever beam (Hwang *et al*. 2004). The reality of the joint is that under the transmitted force by the beam flange, the diaphragm and column flange can move slightly, which create an initial displacement to the system. Thereafter, stress at the joint might not be well predicted.

The displacement of the column flange and diaphragm can be calculated using a superposition of axial stiffness of the individual component. A parallel spring model in Fig. 4 represents the column flange and diaphragm, which attached to fixed sides (leftmost and rightmost) and a rigid body at the middle, subjected to a tension force transmitted from the beam flange. This model was proposed based on the aspect that the column flange and diaphragm, and panel zones relatively deformed. The axial stiffness and displacement of the system can be written as follows.

$$K = K_c + K_d = \frac{D}{\alpha_f b_c^2} + \frac{384 I_d}{5 l_d^3} \tag{6}$$

$$\delta = \frac{F_b}{K} = \frac{M_b}{d_b\left(\frac{D}{\alpha_f b_c^2} + \frac{384 I_d}{5 l_d^3}\right)} \tag{7}$$

where $I_d$ and $l_d$ denote the moment of inertia and length of the diaphragm, respectively. $I_d$ is calculated based on the loading plane from the beam flange.

## 3. Stress predictions

The shear lag stress in steel box member using least-work solution was initially revealed by Reissner (1941, 1946), as concerned with aeronautical problem. For a box beam with stabilized boundary conditions, the stress in the beam flange is non-uniform and distributed in forms of 2nd order polynomial curve. In this investigation, the general function of the longitudinal displacement of the beam flange was considered in high order (*i* order) polynomial curve, as expressed in Eq. (8a).

$$U(x,y) = h\left[w' + \left(1 - \frac{y^i}{b^i}\right)u_1(x)\right] \tag{8a}$$

A FEM study by Kwan (1996) on predicting stress concentration of the core wall revealed that the total stress is significantly affected by the web depth. The web depth enables an increase of the shear lag stress at the edges of the beam flange. Such this issue was concerned, the longitudinal displacement distribution of the beam web given by Lee *et al*. (2001) was considered for the assessment of the shear lag in the box T-joints.

$$U(x,z) = \left[w'z + \left(\frac{z}{h} - \frac{z^3}{h^3}\right)u_2(x)\right] \tag{8b}$$

where $h$ and $b$ are the height and haft width of the beam flange, as shown in Fig. 1(b), respectively. $w$ denotes the flexural displacement of the beam. $x$, $y$, and $z$ represent the coordinate components. $u_1(x)$ and $u_2(x)$ denote the independent displacement density of the beam flange and web corresponding to $x$-axis, respectively.

### 3.1 Least-work solution

The principle of least-work of the bent beam can be utilized to generalize a differential equation through minimizing the potential energy of the system. Considering the top and bottom flanges are identical, the total energy of the system contained the energy due to the load system, strain energy, and the displacement of the column flange can be written in forms of

$$\begin{aligned} U_{TOT} &= \int Mw''dx + \frac{1}{2}\int 2t_w\left(E\varepsilon_w^2 + G\gamma_w^2\right)dxdz \\ &+ \frac{1}{2}\int 2t_f\left(E\varepsilon_f^2 + G\gamma_f^2\right)dxdy + \frac{1}{2}K\delta^2 \end{aligned} \tag{9}$$

where $M$ is the bending moment, and $t_f$ and $t_w$ are the thickness of the beam flange and web, respectively. $E$ and $G$

denote Young's and shear modulus, respectively. $K$ and $\delta$ represent the stiffness and displacement of the column flange, as found in the spring model. The normal ($\varepsilon$) and shear ($\gamma$) strains of the beam can be expressed in the following equations.

$$\varepsilon_f = \frac{\partial U(x,y)}{\partial x},\ \gamma_f = \frac{\partial U(x,y)}{\partial y} \quad \text{for flange} \tag{10a}$$

$$\varepsilon_w = \frac{\partial U(x,z)}{\partial x},\ \gamma_w = \frac{\partial U(x,z)}{\partial z} \quad \text{for web} \tag{10b}$$

By substituting Eqs. (10a)-(10b) into Eq. (9) and minimizing the total potential energy, the equilibrium equations are summarized as follows.

$$M + EIw'' + E\left(\frac{i}{i+1} I_s u_1' + \frac{2}{5h} I_w u_2'\right) = 0 \tag{11a}$$

$$EI_s\left(\frac{i}{i+1} w''' + \frac{2i^2}{(i+1)(2i+1)} u_1''\right) - \frac{i^2}{(2i-1)} \frac{GI_s}{b^2} u_1 = 0 \tag{11b}$$

$$EI_w\left(\frac{2}{5h} w''' + \frac{8}{35h^2} u_2''\right) - GA_w \frac{4}{5h^2} u_2 = 0 \tag{11c}$$

where $I_s = 4bt_f h^2$ and $I_w = (4/3)t_w h^3$. Then, substitute Eqs. (11b)-(11c) into Eq. (11a), the differential equations can be obtained as

$$u_1'' - k_1^2 u_1 - p_1^2 u_2 = u_{01} \tag{12a}$$

$$u_2'' - k_2^2 u_2 - p_2^2 u_1 = u_{02} \tag{12b}$$

where the parameters $k_1$, $p_1$, $u_{01}$, $k_2$, $p_2$, and $u_{02}$ can be found in the appendix A.

The general solutions of the above differential equations can be obtained as

$$u_1(x) = X_{11}C_1 e^{\varphi_1 x} + X_{12}C_2 e^{-\varphi_1 x} + X_{13}C_3 e^{\varphi_2 x} + X_{14}C_4 e^{-\varphi_2 x} - \frac{u_{01}^2}{k_1^2 u_{01} + p_1^2 u_{02}} \tag{13a}$$

$$u_2(x) = X_{21}C_1 e^{\varphi_1 x} + X_{22}C_2 e^{-\varphi_1 x} + X_{23}C_3 e^{\varphi_2 x} + X_{24}C_4 e^{-\varphi_2 x} - \frac{u_{02}^2}{k_2^2 u_{02} + p_2^2 u_{01}} \tag{13b}$$

where $\varphi_1$ and $\varphi_2$ are the corresponding eigenvalues of matrix $A$, as indicated in the appendix A. $X_{11}$, $X_{12}$, $X_{13}$, $X_{14}$ $X_{21}$, $X_{22}$, $X_{23}$, and $X_{24}$ are the corresponding eigenvectors to each eigenvalue. $C_1$, $C_2$, $C_3$, and $C_4$ are the constants obtaining by boundary conditions.

### *3.2 Stress distribution and effective width of the beam flange*

The additional moments at the joint ($x = L$) can be calculated by

$$M_1(L) = \frac{i}{i+1} EI_s u_1'(L) \tag{14a}$$

$$M_2(L) = \frac{2}{5h} EI_w u_2'(L) \tag{14b}$$

The total peak stress at the joint is determined by

$$\sigma_{\max} = \frac{M_T}{I} h = \frac{M_b + M_s}{I} h \tag{15}$$

where $M_b$ denotes the beam bending moment. $M_s$ is the total additional moment due to shear lag ($M_1$+$M_2$). $h$ and $I$ express the height of the beam flange and moment of inertia of the beam, respectively.

As seen in the procedure, the stress evaluation was very complicated due to a necessity of solving the ODE system, and several parameters need to be determined ahead to receiving the stress equation. A more simplified stress evaluation is required for time saving during the preliminary design, and that an empirical method should be provided. The peak stress was simplified using the stress received from least-work solution with an assumption that shear lag occurred in the beam flange alone and modified by a factor $\beta_s$ which represents the shear lag in the beam web. The total stress distribution in the beam flange can be determined as follows.

$$\sigma_L = Eh\left[w'' - \beta_s\left(1 - \frac{y^i}{b^i} - \frac{i}{i+1}\frac{I_s}{I}\right)\left(\frac{P}{k}A_n + \frac{\delta.k}{h}\right)\right] \tag{16a}$$

The peak stress at the joint can be simplified to a combination of bending ($\sigma_b$) and shear lag stress as:

$$\sigma_{\max} = \sigma_b + Eh\frac{i}{i+1}\frac{I_s}{I}\beta_s\left(\frac{P}{k}A_n + \frac{\delta.k}{h}\right) \tag{16b}$$

where, $A_n = \left(\frac{2i+1}{2i}\right)\frac{n}{EI}$, $n = \frac{1}{1 - \left(\frac{2i+1}{2i+2}\right)\frac{I_s}{I}}$,

and $k = \frac{1}{b}\sqrt{\frac{(i+1)(2i+1)}{2(2i-1)}\frac{G}{E}n}$.

The modification factor $\beta_s$ was evaluated using a compatible solution in a parametric study between the stresses in the cantilever beams given by Eqs. (15) and (16b) in relations with the ratio of web depth-to-flange width ($d/2b$). The empirical chart of the factor $\beta_s$ is depicted in Fig. 5 below. The figure shows the values of $\beta_s$ ranges from 0.5-4.

The non-uniform stress can be integrated into an effective sectional area which commonly defines the strength of the beam flange (Tahan *et al.* 1997, Tenchev 1996, Shi and Wang 2016). The effective width of the beam flange at the joint can be calculated following Eq. (17a).

$$b_e = \frac{1}{\sigma_{\max}} \int_0^{b_b} \sigma_L dy \tag{17a}$$

where $\sigma_{max}$ is the maximum stress residing at the edge of the beam flange corresponding to $y = b$. By integrating the stress following to Eq. (16a) and substituting $A_n$, $n$, $k$, and $\delta$, the effective width is simplified as:

$$b_e = \left[1 - \frac{\sqrt{\frac{E}{G}}\left(\frac{\sqrt{4i^2-1}}{i+1}\right) + \frac{b}{L}\left(\frac{2Et_f}{K}\right)\sqrt{\frac{G}{E}}\left(i\sqrt{\frac{2i+1}{2i-1}}\right)\left(\frac{3}{S+3}\right)}{\frac{L}{\beta_s b}\sqrt{\frac{(2i+2)S+3}{S+3}} + \sqrt{\frac{E}{G}}\left(\frac{\sqrt{4i^2-1}}{i+1}\right)\left(\frac{3}{S+3}\right) + \frac{b}{L}\left(\frac{2Et_f}{K}\right)\sqrt{\frac{G}{E}}\left(i\sqrt{\frac{2i+1}{2i-1}}\right)}\right] b_b \quad (17b)$$

where $S$ is the web-to-flange sectional area ratio of the beam ($S = A_w/A_f$). The effective width ratio of the beam flange at the joint is associated with three parameters: the ratio of the beam length-to-haft width of the beam flange ($L/b$), the ratio of the web-to-flange sectional area of the beam ($S$), and axial stiffness of the column flange and diaphragm ($K$). The effective width given in Eq. (17b) is more complex compared with that in Eq. (1). However, the numerical evaluations of the T-joints were assessed to investigate the difference and validity of the effective width calculation including the stress distributions. For the cantilever beam, $b_e$ can be determined by eliminating the column flange flexibility terms in Eq. (17b).

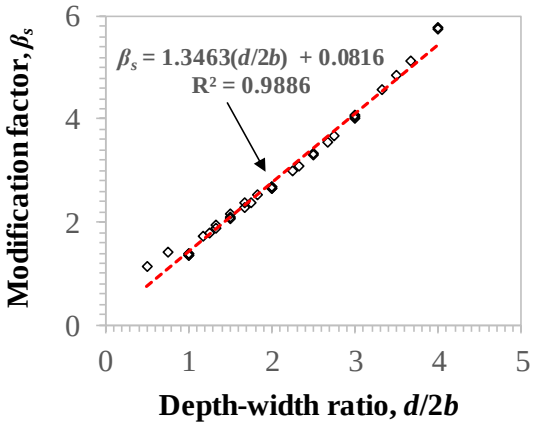


Fig. 5 Modification factor βs for shear lag in box T-joint with diaphragms

## 4. Numerical evaluations

The box T-joints were numerically performed to evaluate the displacement of the column flange and stress distributions of the beam flange at the joint. The study also included the parametric effects on the stress due to the beam section properties. This procedure utilized the finite element method (FEM) assisted by a computer software Abaqus (Abaqus/CAE 2017). The FEM results were carried out to compare and validate the column flange flexibility and stress in the preceding predictions. Nonetheless, using FEM requires comprehensive modeling which is able to assure the reliability of the results. Such this investigation involved with finite element (FE) modeling, the FE validation of the existing experiment is necessary. As much as the FE modeling was guaranteed to be used, expanding the numerical study of the box T-joint could be provided.

### *4.1 FE modeling and validation*

A 3D solid 8-node element (C3D8-R) was used in this numerical study, as revealed by Serrano-López *et al.* (2016) and Moazed *et al.* (2009) that the solid element provides more reliable results compared with the shell element. For the investigation of the column flange flexibility, the plate-to-box column connections were built with triple symmetric geometry and modeled as one eighth of the actual connection. However, the full connection model was implemented for the box T-joints. The material nonlinearities were also included to represent the actual characteristics of the steel. The stress-strain curve of the steel was modeled as multi-linear isotropic behavior with strain hardening corresponding to JSCE (JSCE 2007) for monotonic loading. The combined isotropic-kinematic hardening was utilized for cyclic loading. It was noted that welding was not included in the modeling. A mesh size of one-half and one time of the element thickness was applied to the thickness of the connection component and to

Table 1 Section and material properties of the selected specimens (Sasaki *et al.* 2001)

| Type | Beam/column | | | | | | Stiffener | | |
|---|---|---|---|---|---|---|---|---|---|
| | $b_0$ | $d$ | $t_f$ | $t_w$ | $F_{yf}$ | $F_{yw}$ | $h_s$ | $t_s$ | $F_{ys}$ |
| T-joint | 312 | 309 | 9 | 8 | 293 | 299 | 80 | 10 | 288 |

Note: all geometric dimensions in mm. Specified yield stress in MPa.

portions where the characteristic components were considered, respectively.

The comparison with the experiment results was delivered in order to validate the FE modeling. A test of a built-up stiffened box T-joint (test No. 1) by Sasaki *et al.* (2001) was selected to numerically perform under static and cyclic bending. The test No. 1 consists of a beam with the length of 1350 mm, which connected to a column with the length of 2900 mm. Stiffeners were used and located at the mid-width of the flange and web of the beam and column, as to prevent local buckling. One end of the column was fixed while another end was restrained by a pinned support. A pre-compression load of 294 kN was applied to the beam. In addition, beam of the T-joint subjected to a lateral point load placed at the beam free end. The section and material properties of the selected test sample are summarized in Table 1 below.

The results of the box T-joint were compared with the test in terms of the static load-displacement relations and stress distribution at 20 mm from the column face. Fig. 6 shows the comparison results. The static load-displacement was constructed in accordance with the peak loads at each cycle in the cyclic test results. Meanwhile, the stress distribution at 20 mm from the column face was also provided when the lateral load reached a value of 147 kN. The comparison showed that the cyclic performances

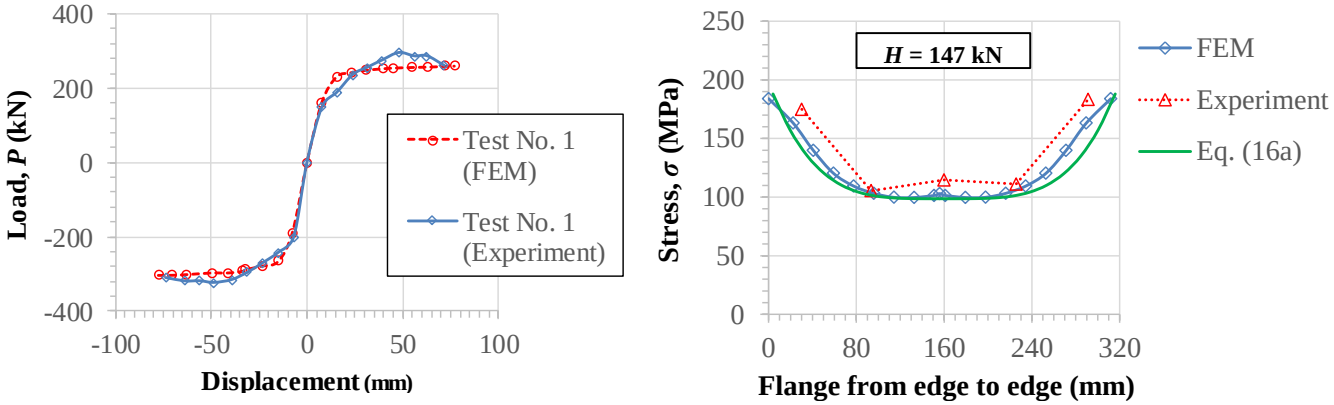


(a) Static load-displacement curve (b) Stress distribution on beam flange

Fig. 6 FEM and experiment comparison

maintained fairly matched load-displacement relations. Furthermore, the stress distributions given by FEM and Eq. (16a) were well comparable to settle a generalized FEM study.

The results of the box T-joint were compared with the test in terms of the static load-displacement relations and stress distribution at 20 mm from the column face. Fig. 6 shows the comparison results. The static load-displacement was constructed in accordance with the peak loads at each cycle in the cyclic test results. Meanwhile, the stress distribution at 20 mm from the column face was also provided when the lateral load reached a value of 147 kN. The comparison showed that the cyclic performances maintained fairly matched load-displacement relations. Furthermore, the stress distributions given by FEM and Eq. (16a) were well comparable to settle a generalized FEM study.

### *4.2 Flexibility of column flange*

The flexibility of column flange presented in section 2.1 is defined by the coefficient $\alpha_f$, which obtained based on the effective width. For Eq. (17b), the effective width can be determined only if the column flange deflection is known. In this FEM study, an evaluation of column flange flexibility of the box T-joint was provided. As the loads were transmitted through the beam flanges, the investigation was carried out by simulating the box T-joint as a plate-to-box column connection, which the plate subjected to tension force. Due to the triple symmetric geometries, the analytical connection was simulated as one eight of the actual connection, as shown in Fig. 7.

This study consists of 35 connection models in which the column flange width and thickness were respectively varied from 100 to 1000 mm and 4 to 40 mm, corresponding to the width-to-thickness ratio ($2\gamma = b_c/t_c$) from 15 to 50. The pull plate with the thickness ratio ($t_c/t_p$) ranged from 0.4 to 1 was considered in the investigation. The concept used to evaluate the column flange flexibility was to construct the load-displacement relations of the column flange under the tension force of the plate. Once the load-displacement relations were known, the compatibility of the initial stiffness between FEM and Eq. (4) was used to determine the flexibility coefficient of the column flange ($\alpha_f$). The relationship between $\alpha_f$ and $2\gamma$ was plotted and can be seen in Fig. 8(a) below. As observed, the flexibility of the column flange ($\alpha_f$) degraded relatively to the greater column width-to-thickness ratio ($2\gamma$). According to Eq. (1), the effective width of the column flange, which established the flexibility as shown in Fig. 3, can be written in forms of the column width-to-thickness ratio ($2\gamma$), and vi-versa. The comparison of $\alpha_f$ between FEM and the effective width of the column flange is depicted in Fig. 8(b). The empirical values given by FEM provided the nearest characteristics compared with the effective width method when the thicknesses of the beam and column equaled to 0.75-1. In contrast, different $\alpha_f$ was observed when the column-to-beam thickness ratio was not equal to a value in between 0.75-1. On the other hand, all the curves started to converge when $2\gamma$ came next to 50. For this observation, the deflection of the column flange can be calculated using either the empirical values of $\alpha_f$ illustrated in Fig. 8(a) or the effective width when $t_c/t_b = 0.75$-1.

### *4.3 Stress evaluation*

The static performance assessment of the box T-joint considered the effects of column flange and diaphragm on the stress distribution in the beam flange. The basic joint model formed of a 300x300x8 mm-box column and beam without using diaphragms subjected to in-plane bending, in which a point load $P$ = 50 kN located at the free end of the beam and expected to perform in an elastic manner. The bending stress ($\sigma_b$) was calculated to be 90.37 MPa. Two extending cases included the joint with full and hole internal diaphragms. The thickness of the diaphragm was selected to be 8 mm, as equal to the beam flange thickness. The circular and square holes of 100 mm in diameter and width located at the center of the diaphragm. The presence of a hole in the diaphragm provided feasibility for concrete filling in the box column or inspection. Such this investigation involved with FEM, the stress distribution was brought into comparison with Eq. (16a) with a modification factor $\beta_s$ as shown in Fig. 5.

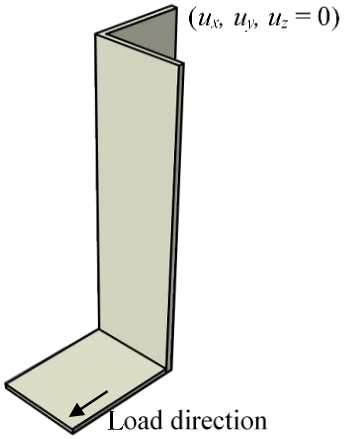


(a) Plate-to-box column model

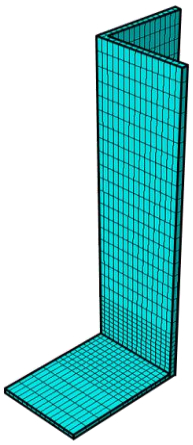

(b) Meshing

Fig. 7 Plate-to-box column connection and meshing

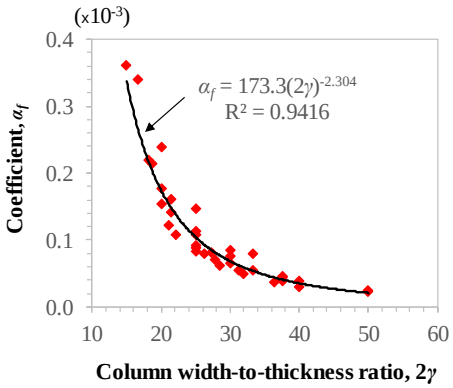


(a) Coefficient αf by FEM

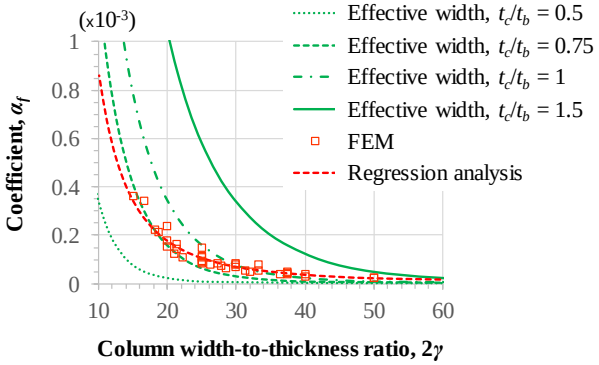


(b) Comparison of αf by FEM and Eq. (1)

Fig. 8 Flexibility coefficient of column flange

The von Mises stress contours of the box T-joints in this study are depicted in Fig. 9. The stress reached maximum at the edges of the beam flange and degraded to minimum at the mid-width of the flange. The basic T-joint, as seen in Fig. 9(a), delivered the highest stress compared with the T-joints in which the column flange was restrained by the diaphragms. In addition, the diaphragm hole, which caused an increase in deflection of the column flange, also affected the stress increase at the edge of the beam flange, as observed in Figs. 9(c)-(d). In every aspect, the diaphragms are very crucial in use to reduce the stress concentration at the edges of the beam flange, as it improved the rigidity of the column flange.

The normal tensile stress distributions along the width of the beam flange at the joint region were plotted and compared with Eq. (16a), as shown in Fig. 10. The stresses given by Eq. (16a) were also provided based on the assumptions of the longitudinal displacement of the beam flange using $4^{th}$, $6^{th}$, and $8^{th}$ order polynomial curves ($i$ = 4, 6, 8). In this study, for all T-joints (with/without diaphragms) with $i$ = 4 and 6, the stresses by FEM and Eq. (16a) delivered well compatible values at the edges of the beam flange. For the basic T-joint (without diaphragm), the stress was distributed without considering the effect of shear lag in the web, as fairly acceptable by the FEM. It was also observed in Fig. 10(b) that Eq. (16a) and the FEM provided almost identical stress distributions. However, significant differences of the stresses were observed at mid-width of the beam flange of the T-joint with hole diaphragm, as seen in Fig. 10(c). This occurrence was due to the over-predicted deflection of the column flange, which able to increase stress at the edge and decrease at mid-width of the beam flange. The above situation is related with the hole diaphragm for which the deflection was calculated based on the moment inertia at where the hole located. More importantly, since the stress at mid-width of the beam flange were not much necessary for the preliminary design, evaluating the stress at the edge of the beam flange using Eq. (16a) with $4^{th}$ order polynomial function of longitudinal displacement was alternatively satisfied.

### *4.4 Peak stress and effective width of the beam flange*

Since the peak stress at the edge and effective width of the beam flanges have been preferred for design and check, this FE parametric study evaluated the peak stress and compared with Eq. (16b). The comparison of effective width between Eqs. (1) and (17b) was also carried out. This investigation was divided into 4 series; each series consisted

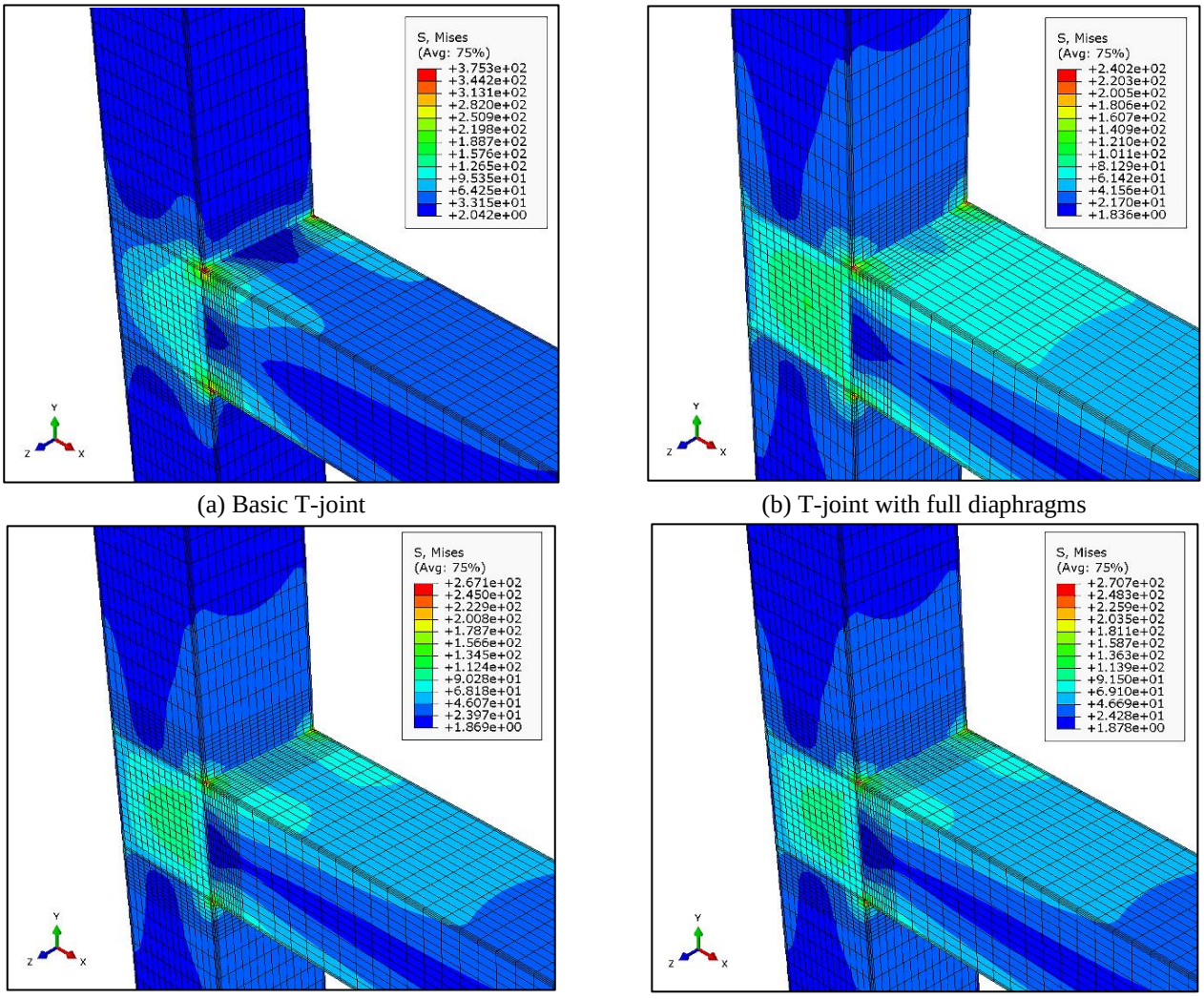


(a) Basic T-joint (b) T-joint with full diaphragms

(c) T-joint with 100 mm-circular hole diaphragms (d) T-joint with 100 mm-square hole diaphragms

Fig. 9 von Mises stress developed in the box T-joints

Table 2 Summary of geometric properties and loadings of the box T-joint models

| Series | Model | Column | Beam | | | Diaphr. | Loading | |
|---|---|---|---|---|---|---|---|---|
| | | $b_c$ x $t_c$ | $b_b$ x $d_b$ x $t_b$ | $S=A_w/A_f$ | $L_b$ | $t_d$ | $P$ (N) | $\sigma_b$ (MPa) |
| 200 | B200x150x6 | 200x6 | 200x150x6 | 0.74 | 1600 | 6 | 13000 | 103.62 |
| | B200x200x6 | 200x6 | 200x200x6 | 1.00 | 1600 | 6 | 18000 | 98.61 |
| | B200x300x6 | 200x6 | 200x300x6 | 1.52 | 1600 | 6 | 32000 | 101.43 |
| 300 | B300x200x8 | 300x8 | 300x200x8 | 0.66 | 1600 | 8 | 33000 | 100.58 |
| | B300x300x8 | 300x8 | 300x300x8 | 1.00 | 1600 | 8 | 55000 | 99.41 |
| | B300x450x8 | 300x8 | 300x450x8 | 1.51 | 1600 | 8 | 95000 | 99.62 |
| 400 | B400x300x16 | 400x16 | 400x300x16 | 0.74 | 2000 | 16 | 103000 | 100.05 |
| | B400x400x16 | 400x16 | 400x400x16 | 1.00 | 2000 | 16 | 151000 | 100.00 |
| | B400x600x16 | 400x16 | 400x600x16 | 1.52 | 2000 | 16 | 263000 | 99.95 |
| 600 | B600x400x20 | 600x20 | 600x400x20 | 0.66 | 2400 | 20 | 213000 | 100.19 |
| | B600x600x20 | 600x20 | 600x600x20 | 1.00 | 2400 | 20 | 361000 | 99.91 |
| | B600x800x20 | 600x20 | 600x800x20 | 1.34 | 2400 | 20 | 532000 | 99.93 |

Note: all geometric dimensions in mm.

Table 3 Normalized peak stress and effective width of the beam flange in the box T-joint without diaphragm

| Series | Model | *d/2b* | Normalized stress, $\sigma_{max}/\sigma_b$ | | | Effective width, $b_e$ | |
|---|---|---|---|---|---|---|---|
| | | | FEM | Eq. (16b) | Diff (%) | Eq. (1) | Eq. (17b) |
| 200 | B200x150x6 | 0.74 | 2.78 | 3.18 | -14.59 | 60 | 87 |
| | B200x200x6 | 1.00 | 3.05 | 3.04 | 0.43 | 60 | 96 |
| | B200x300x6 | 1.52 | 3.04 | 2.84 | 6.41 | 60 | 110 |
| 300 | B300x200x8 | 0.66 | 2.92 | 3.22 | -10.19 | 80 | 124 |
| | B300x300x8 | 1.00 | 2.92 | 3.01 | -2.98 | 80 | 143 |
| | B300x450x8 | 1.51 | 2.89 | 2.81 | 2.79 | 80 | 164 |
| 400 | B400x300x16 | 0.74 | 2.96 | 3.39 | -14.68 | 160 | 164 |
| | B400x400x16 | 1.00 | 2.98 | 3.23 | -8.36 | 160 | 183 |
| | B400x600x16 | 1.52 | 3.09 | 3.02 | 2.21 | 160 | 212 |
| 600 | B600x400x20 | 0.66 | 3.12 | 3.38 | -8.32 | 200 | 237 |
| | B600x600x20 | 1.00 | 3.31 | 3.16 | 4.56 | 200 | 275 |
| | B600x800x20 | 1.34 | 3.36 | 3.01 | 10.53 | 200 | 304 |

Note: $\beta_s = 1$ for the box T-joint without diaphragm.

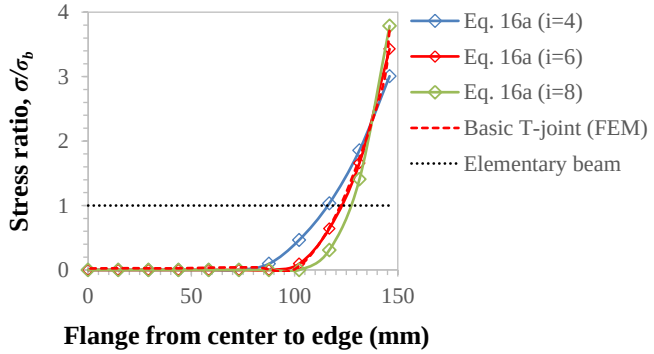


(a) Basic T-joint without diaphragm

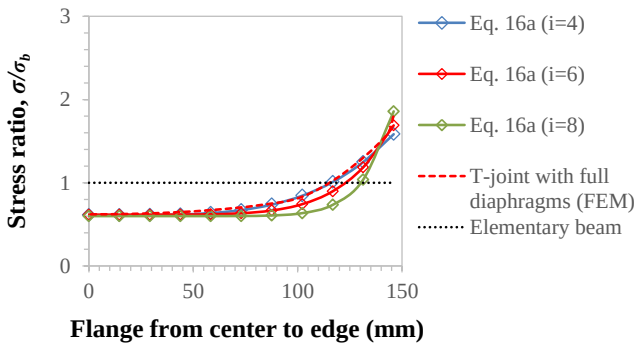


(b) T-joint with full diaphragms

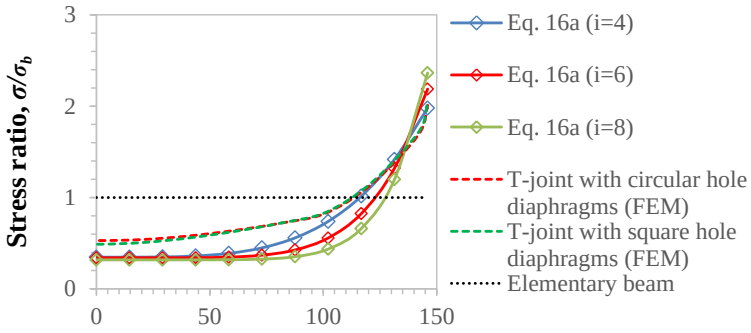


(c) T-joint with 100 mm-hole diaphragms

Fig. 10 Stress distribution in the beam flange

of 3 box T-joint models, and the size and thickness of the column and beam were changed. The column length was set to be 2 m for series 200 and 300, 2.6 m for series 400, and 3.2 m for series 600. A point load equivalent to a bending stress of 100 MPa was applied at the free end of the beam. The box T-joint models presented in this study are summarized in Table 2 below.

The peak stress was measured at the junction between the web and flange of the beam and normalized by the bending stress. It can also be calculated using Eq. (16b) by replacing $y = b$, which physically means the peak stress was represented by the bending moment and additional moment due to shear lag. The 4$^{th}$-order polynomial function of the longitudinal displacement of the beam flange was considered for evaluating the stress and effective width using Eqs. (16b) and (17b). Tables 3-4 describe the normalized peak stress and the effective width of the beam flange in the box T-joint with and without diaphragms, respectively.

Table 4 Normalized peak stress and effective width the beam flange in the box T-joint with full diaphragms

| Series | Model | *d/2b* | $\beta_s$ | Normalized stress, $\sigma_{max}/\sigma_b$ | | | | | $b_e$ |
|---|---|---|---|---|---|---|---|---|---|
| | | | | FEM | Eq. (16b) | Diff (%) | Okumura | Diff (%) | Eq. (17b) |
| 200 | B200x150x6 | 0.74 | 1.08 | 1.48 | 1.45 | 2.11 | 1.13 | 23.54 | 144 |
| | B200x200x6 | 1.00 | 1.43 | 1.64 | 1.55 | 5.35 | 1.12 | 31.56 | 139 |
| | B200x300x6 | 1.52 | 2.12 | 1.87 | 1.73 | 7.78 | 1.10 | 41.08 | 133 |
| 300 | B300x200x8 | 0.66 | 0.97 | 1.55 | 1.45 | 6.16 | 1.14 | 26.38 | 212 |
| | B300x300x8 | 1.00 | 1.43 | 1.69 | 1.59 | 5.83 | 1.12 | 33.71 | 199 |
| | B300x450x8 | 1.51 | 2.12 | 1.87 | 1.77 | 5.08 | 1.10 | 41.00 | 188 |
| 400 | B400x300x16 | 0.74 | 1.08 | 1.50 | 1.50 | 0.18 | 1.13 | 24.78 | 274 |
| | B400x400x16 | 1.00 | 1.43 | 1.62 | 1.61 | 0.80 | 1.12 | 31.09 | 262 |
| | B400x600x16 | 1.52 | 2.13 | 1.86 | 1.80 | 2.98 | 1.10 | 40.75 | 247 |
| 600 | B600x400x20 | 0.66 | 0.96 | 1.64 | 1.49 | 9.10 | 1.14 | 30.68 | 408 |
| | B600x600x20 | 1.00 | 1.43 | 1.86 | 1.64 | 11.59 | 1.12 | 39.77 | 380 |
| | B600x800x20 | 1.34 | 1.89 | 2.00 | 1.78 | 11.34 | 1.11 | 44.77 | 362 |

As observed in Table 3, the box T-joints without diaphragm, which were evaluated by FEM, provided almost identical normalized peak stresses compared with Eq. (16b). This circumstance did not require to modify the shear lag stress induced by the web. The box T-joints without diaphragm exercised the very high stress concentration at the edge of the beam flange. In table 4 as the full diaphragms were settled, the stress concentration degraded significantly from 40 to 60%. More importantly, it was observed that the peak stress ratios grew respectively to the deep webs, which admitted by both the FEM and Eq. (16b). The peak stress given by Eq. (16b) was simple to calculate and more accurate compared to Okumura' equation. Furthermore, the effective width for the box T-joint without diaphragm using Eq. (17b) went down nearest to Eq. (1) when the shorter web depth was used. Unlike the box T-joint without diaphragm, the presence of diaphragms developed large effective area for the beam flange, as meant the strength of the connection improved significantly.

## 5. Summary and conclusions

The theoretical and numerical evaluations of stress and effective width due to shear lag in the box T-joints under in-plane bending were conducted in this study. Using least-work solution with the assumed longitudinal displacement function of the beam flange and web and considering the effect of column flange flexibility, the normal stress distribution and effective width were evaluated theoretically. The flexibility of the box T-joint, which caused by two main components, such as the column flange and diaphragms, is represented by an axial spring model and contributed to stress distribution in the beam flange. Thereafter, the finite element assessment was extensively conducted to check the validity of shear lag stress equation. The main findings in this study can be concluded as follows.

- The flexibility of the column flange was very sensitive in causing high stress concentration at the edges of the beam flange. To reduce such that uneven circumstance, the diaphragms were introduced into the box T-joint. The full diaphragms (no hole), which have thickness equal to that of the beam flange, were able to diminish the stress concentration from 40 to 60%.
- The evaluation of stress required the initial displacement of the beam flange, which was predicted based on the column flange and diaphragm deflection. The deflection of the column flange can be calculated using the effective width method, as given in Eq. (4). However, an empirical chart, as shown in Fig. 8(a) can also be used to evaluate the flexibility coefficient $\alpha_f$, following the calculation of the deflection of the column flange.
- Considering the effects of column flange and diaphragm flexibility, the approach provided more well-predicted stress distribution compared with the assumption that a box T-joint behaves as cantilever beam which maintained under-predicted peak stress. Using $4^{th}$ or $6^{th}$ order polynomial function for the longitudinal displacement of the beam flange was acceptable for evaluation of the stress in the box T-joint with or without diaphragms.
- However, the stress and effective width of the beam flange in the box T-joint with diaphragms were significantly affected by the ratio of web depth-to-flange width of the beam (*d/2b*). The peak stresses increased corresponding to the deep web and resulted as the smaller effective width. A simplified method was established to easily calculate the shear lag stress. The method required to calculate the stress derived by an assumption that shear lag occurred in the beam flange alone, and multiply to a modification factor ($\beta_s$) that represented the effect of shear lag in the beam web.

## Acknowledgments

Many thanks are given to Japan International Cooperation Agency (JICA) for financial support under AUN/SEED Net Program Phase 3.

## References


Abaqus/CAE (2017), *User's Manual, Dassault Systemes*; Vélizy-Villacoublay, France.

AIJ (2008), *Recommendations for Design and Construction of Concrete Filled Steel Tubular Structures*, Architectural Institute of Japan; Tokyo, Japan.

ANSI/AISC 360-10 (2010), Specification for Structural Steel Buildings, American Institute of Steel Construction; Chicago, IL, USA.

Chang, S.T. and Zheng, F.Z. (1987), "Negative shear lag in cantilever box girder with constant depth", *J. Struct. Eng.*, **113**(1), 20-35.
https://doi.org/10.1061/(ASCE)0733-9445(1987)113:1(20).

Chen, J., Shen, S.L., Yin, Z.Y. and Horpibulsuk, S. (2014), "Closed-form solution for shear lag with derived flange deformation function", *J. Constr. Steel Res.*, **102**(2014), 104-110. https://doi.org/10.1016/j.jcsr.2014.07.003.

CIDECT 9 (2004), *Design Guide for Structural Hollow Section Column Connections*, Committee for International Development and Education on Construction of Tubular Structures, Köln, Germany.

Dezi, L. and Mentrasti, L. (1985), "Nonuniform bending-stress distribution (shear lag)", *J. Struct. Eng.*, **111**(12), 2675-2690. https://doi.org/10.1061/(ASCE)0733-9445(1985)111:12(2675).

Eurocode 3 (2005), Design of steel structures - Part 1-8: Design of joints, European Committee for Standardization; Brussels, Belgium.

Fadden, M. and McCormick, J. (2013), "Evaluation of HSS-to-HSS Moment Connections for Seismic Applications", *Structures Congress 2013*, Pittsburgh, PA, USA, May. https://doi.org/10.1061/9780784412848.204.

Hwang, W.S., Kim, Y.P., and Park, Y.M. (2004), "Evaluation of shear lag parameters for beam-to-column connections in steel piers", *Struct. Eng. Mech.*, **17**(5), 691-706. https://doi.org/10.12989/SEM.2004.17.5.691.

JRA (2002), Specification for Highway Bridges, Part II: Steel Bridge Design, Japan Road Association; Japan.

JSCE (2007), Standard Specifications for Steel and Composite Structures, Japan Society of Civil Engineers; Japan.

Kristek, V., Evan, H.R., and Ahmad, M.K.M. (1990), "A shear lag analysis for composite box girders", *J. Constr. Steel Res.*, **16**(1), 1-21. https://doi.org/10.1016/0143-974X(90)90002-X.

Kwan, A.K.H. (1996), "Shear lag in shear/core walls", *J. Struct. Eng.*, **122**(9), 1097-1104. https://doi.org/10.1061/(ASCE)0733-9445(1996)122:9(1097).

Lee, K.-K., Loo, Y.-C. and Guan, H. (2001), "Simple analysis of framed-tube structures with multiple internal tubes", *J. Struct. Eng.*, **127**(4), 450-460. https://doi.org/10.1061/(ASCE)0733-9445(2001)127:4(450).

Lin, Z. and Zhao, J. (2011), "Least-work solutions of flange normal stresses in thin-walled flexural members with high-order polynomial", *Eng. Struct.*, **33**(10), 2754-2761. http://dx.doi.org/10.1016/j.engstruct.2011.05.022.

Miki, C. and Sasaki, E. (2005), "Fracture in steel bridge piers due to earthquake", *Int. J. Steel Struct.*, **5**(2), 133-140.

Moazed, R., Szyszkowski, W.-Ã., and Fotouhi, R. (2009), "The in-plane behaviour and FE modeling of a T-joint connection of thin-walled square tubes", *Thin-Walled Struct.*, **47**(6-7), 816-825. https://doi.org/10.1016/j.tws.2009.01.006.

Mohammadnejad, M. and Kazemi, H.H. (2018), "A new and simple analytical approach to determining the natural frequencies of framed tube structures", *Struct. Eng. Mech.*, **65**(1), 111-120. https://doi.org/10.12989/sem.2018.65.1.111.

Okumura, T. and Ishizawa, N. (1968), "The design of knee joints for rigid steel frames with thin walled section", *Trans. Japan Soc. Civ. Eng.*, **1968**(153), 1-18. https://doi.org/10.2208/jscej1949.1968.153_1.

Reissner, E. (1941), "Least-work solutions of shear lag problems", *J. Aeronaut. Sci.*, **8**(7), 284-291. https://doi.org/10.2514/8.10712.

Reissner, E. (1946), "Analysis of shear lag in box beams by the principle of minimum potential energy", *Q. Appl. Math.*, **4**(3), 268-278. https://www.jstor.org/stable/43633559.

Sasaki, E., Takahashi, K., Ichikawa, A., Miki, C. and Natori, T. (2001), "Influences of stiffening methods on elasto-plastic behavior of beam-to-column connections of steel rigid frame piers", *Proc. the Japan Soc. of Civ. Eng.*, **689**(57), 201-214. https://doi.org/10.2208/jscej.2001.689_201.

Serrano-López, M.A., López-Colina, C., González, J. and López-Gayarre, F. (2016), "A simplified FE simulation of welded I beam-to-RHS column joints", *Int. J. Steel Struct.*, **16**(4), 1095-1105. https://doi.org/10.1007/s13296-016-0028-5.

Shi, Q.X. and Wang, B. (2016), "Simplified calculation of effective flange width for shear walls with flange", *Struct. Design Tall Spec. Build.*, **25**(12), 558-577. https://doi.org/10.1002/tal.1272.

Tahan, N., Pavlovic, M.N., and Kotsovos, M.D. (1997), "Shear-lag revisited: the use of single fourier series for determining the effective breadth in plated structures", *Comput. Struct.*, **63**(4), 759-767. https://doi.org/10.1016/S0045-7949(96)00065-X.

Tanabe, A. (2005), "Fatigue Retrofitting of Steel Bridge Frame Piers with High Seismic Performance", Ph.D. Dissertation; Tokyo Institute of Technology, Tokyo, Japan.

Tenchev, R.T. (1996), "Shear lag in orthotropic beam flanges and plates with stiffeners", *Int. J. Solids Struct.*, **33**(9), 1317-1334. http://dx.doi.org/10.1016/0020-7683(95)00093-3.

Timoshenko, S. and Woinowsky-Krieger, S. (1987), *Theory of Plates and Shells*, McGraw-Hill, Inc., Singapore.

Winter, G. (1940), "Stress Distribution in and Equivalent Width of Flanges of Wide, Thin-Walled Steel Beams", NACA Technical Note No. 784; Cornell University, U.S.A.

Zhou, W.-W., Jiang, L.Z., Liu, Z.J., and Liu, X.J. (2012), "Closed-form solution to thin-walled box girders considering effects of shear deformation and shear lag", *J. Cent. South. Univ.*, **19**(9), 2650-2655. https://doi.org/10.1007/s11771-012-1323-8.


*CC*

## Appendix A: least-work solution for shear lag in the box T-joints

The total energy of the box T-joint system can be written in forms of

$$U_{TOT} = \int Mw''dx + \frac{1}{2}\int 2t_w\left(E\varepsilon_w^2 + G\gamma_w^2\right)dxdz + \frac{1}{2}\int 2t_f\left(E\varepsilon_f^2 + G\gamma_f^2\right)dxdy + \frac{1}{2}K\delta^2 \tag{A-1}$$

Substitute Eqs. (10a)-(10b) into Eq. (9), the total energy of the system becomes,

$$\begin{aligned} U_{TOT} = {} & \int Mw''dx + \frac{1}{2}\int EI_w w''^2 dx \\ & + \int E\left(\frac{i}{i+1}I_s u_1' + \frac{2}{5h}I_w u_2'\right)w''dx \\ & + \int\left(\frac{i^2}{(i+1)(2i+1)}I_s u_1'^2 + \frac{4}{35h^2}I_w u_2'^2\right)dx \\ & + \int G\left(\frac{i^2}{2(2i-1)}\frac{I_s u_1^2}{b^2} + \frac{2}{5h^2}A_w u_2^2\right)dx \\ & + \frac{1}{2}\int GA_w w'^2 dx + \frac{1}{2}K\delta^2 \end{aligned} \tag{A-2}$$

Minimize the total energy, the equilibrium equations are summarized as:

$$M + EIw'' + E\left(\frac{i}{i+1}I_s u_1' + \frac{2}{5h}I_w u_2'\right) = 0 \tag{A-3}$$

$$EI_s\left(\frac{i}{i+1}w''' + \frac{2i^2}{(i+1)(2i+1)}u_1''\right) - \frac{i^2}{(2i-1)}\frac{GI_s}{b^2}u_1 = 0 \tag{A-4}$$

$$EI_w\left(\frac{2}{5h}w''' + \frac{8}{35h^2}u_2''\right) - GA_w\frac{4}{5h^2}u_2 = 0 \tag{A-5}$$

Then, substitute Eqs. (A-3)-(A-4) into Eq. (A-2), the differential equations can be obtained as

$$u_1'' - k_1^2 u_1 - p_1^2 u_2 = u_{01} \tag{A-6}$$

$$u_2'' - k_2^2 u_2 - p_2^2 u_1 = u_{02} \tag{A-7}$$

where, $n_1 = \dfrac{1}{1-\left(\dfrac{2i+1}{2i+2}\right)\dfrac{I_s}{I} - \dfrac{7}{10}\dfrac{I_w}{I}}$,

$$k_1 = \frac{1}{b}\sqrt{\frac{(i+1)(2i+1)}{2(2i-1)}\frac{G}{E}\left(1-\frac{7}{10}\frac{I_w}{I}\right)n_1},$$

$$p_1 = \frac{1}{b}\sqrt{\frac{7}{5}\frac{(2i+1)}{2i}\frac{G}{E}\frac{A_w}{Ih}n_1},\quad u_{01} = \frac{Q}{EI}\frac{(2i+1)}{2i}n_1,$$

$$n_2 = n_1,\quad k_2 = \frac{1}{b}\sqrt{\frac{7}{2}\frac{G}{E}\frac{A_w}{I_w}\left(1-\frac{(2i+1)}{2i}\frac{I_s}{I}\right)n_2},$$

$$p_2 = \frac{1}{b}\sqrt{\frac{7h}{4}\frac{i(2i+1)}{2(2i-1)}\frac{G}{E}\frac{I_s}{I}n_2},\quad u_{02} = \frac{Q}{EI}\frac{7h}{4}n_2,$$

and $Q$ is the beam shear force.

To solve 2nd order ODE systems as shown in Eqs. (33) and (34), let $u_1' = u_3$ and $u_2' = u_4$, the 1st order ODE system can be written as:

$$u_1' - u_3 = 0 \tag{A-8}$$

$$u_2' - u_4 = 0 \tag{A-9}$$

$$u_3' - k_1^2 u_1 - p_1^2 u_2 = u_{01} \tag{A-10}$$

$$u_4' - k_2^2 u_2 - p_2^2 u_1 = u_{02} \tag{A-11}$$

Let a matrix $A$,

$$A = \begin{bmatrix} 0 & 0 & 1 & 0 \\ 0 & 0 & 0 & 1 \\ k_1^2 & p_1^2 & 0 & 0 \\ p_2^2 & k_2^2 & 0 & 0 \end{bmatrix} \tag{A-12}$$

Eigenvalues of matrix $A$ can be expressed as

$$\phi = \begin{bmatrix} \pm\sqrt{\frac{1}{2}\left(k_1^2 + k_2^2 - \sqrt{\left(k_1^2 + k_2^2\right)^2 - 4\left(k_1^2 k_2^2 - p_1^2 p_2^2\right)}\right)} \\ \pm\sqrt{\frac{1}{2}\left(k_1^2 + k_2^2 + \sqrt{\left(k_1^2 + k_2^2\right)^2 - 4\left(k_1^2 k_2^2 - p_1^2 p_2^2\right)}\right)} \end{bmatrix} \tag{A-13}$$